AN ABSTRACT OF THE THESIS OF

Adam P. Damiano for the degrees of Honors Baccalaureate of Science in Mechanical Engineering and Honors Baccalaureate of Arts in International Studies in Mechanical Engineering presented on May 28, 2013. Title: Empirical Analysis of Two-Phase Confined Impinging Jet Heat Transfer.

Abstract Approved:

_____

Deborah V. Pence

Advances in electronics fabrication, coupled with the demand for increased computing power, have driven the demand for innovative cooling solutions to dissipate waste heat generated by these devices. To meet future demands, research and development has focused on robust two-phase heat transfer devices. A confined impinging jet is explored as a means of utilizing two-phase heat transfer. How this technology may be applicable to desalination is highlighted.

The test configuration consists of a 4 mm diameter jet of water, at a subcooled temperature of 10 degrees Celsius, which impinges on a 38 mm diameter heated aluminum surface. Experimental parameters include inlet mass fluxes ranging from 200 to 400 kg/m^2-s, confinement gap height to nozzle diameter ratios from 0.125 to 0.5, and input heat fluxes from 5 to 50 W/cm^2. The influence of the testing parameters on the heat transfer performance is assessed. Conditions of the heater surface strongly influence

heat transfer performance. Procedures were established to prepare an aluminum heating surface with repeatable surface characteristics. Existing confined impinging jet heat transfer correlations based on two-phase inlet conditions were modified for single-phase inlet conditions with two-phase flow within the confinement region.

Key Words: Confined Impinging Jets, Heat Sinks, Flow Boiling, Desalination.

Corresponding e-mail address: adam@adamdamiano.com

Empirical Analysis of Two-Phase Confined Impinging Jet Heat Transfer

by

Adam P. Damiano

A THESIS

submitted to

Oregon State University

University Honors College

in partial fulfillment of
the requirements for the
degrees of

Honors Baccalaureate of Science in Mechanical Engineering

Honors Baccalaureate of Arts in International Studies in Mechanical Engineering

Presented May 28, 2013
Commencement June 2013

Honors Baccalaureate of Science in Mechanical Engineering and Honors Baccalaureate of Arts in International Studies in Mechanical Engineering thesis of Adam P. Damiano presented on May 28, 2013.

APPROVED:

_____

Mentor, representing Mechanical Engineering

_____

Committee Member, representing Mechanical Engineering

_____

Committee Member, representing International Studies

_____

Head of the School of Mechanical, Industrial, and Manufacturing Engineering

_____

Dean, University Honors College

I understand that my project will become part of the permanent collection of Oregon State University, University Honors College. My signature below authorizes release of my project to any reader upon request.

_____

Adam P. Damiano, Author

ACKNOWLEDGEMENTS

I would like to thank my parents, Phil Damiano and Karen Johannes, for their unstinting support of my academic pursuits. I would also like to extend thanks to my sister, Lindsay Damiano, for the motivation that she gave me throughout my undergraduate studies. I would thank my advisor, Dr. Deborah Pence, for her guidance over the last two years and for providing me with the opportunity to conduct research at the undergraduate level. I would also like to thank Dr. James Liburdy and Nick Fleury for serving on my committee and for their assistance in the thesis process. I express sincere gratitude to my labmates, Nick Cappello and Christopher Stull, for their aid and companionship. I would also like to thank Mike Sabo for laying the foundation upon which this research project was possible and for allowing me to use his figures in this thesis. Additionally, I would like to thank Xiaoliang He, Randall Fox, and Saran Salakijs for the insight that they offered. Finally, I would like to thank the brothers of the Kappa Omicron Chapter of The Fraternity of Phi Gamma Delta for the endless ways in which they have contributed towards my academic achievements at Oregon State University.

TABLE OF CONTENTS

TABLE OF CONTENTS (Continued)

LIST OF FIGURES

LIST OF FIGURES (Continued)

NOMENCLATURE

A	Area (m^2)
c_p	Specific heat (J/kg-K)
d	Diameter (m)
G	Mass flux (kg/m^2-s)
g	Gravitational constant (m/s^2)
H	Nozzle-to-surface spacing (m)
h	Heat transfer coefficient (W/m^2-K)
i	Enthalpy (J/kg)
i_{fg}	Heat of vaporization (J/kg)
k	Thermal conductivity (W/m-K)
L	Nozzle length (m)
Nu	Nusselt number
P	Pressure (Pa)
Pr	Prandtl number
q	Electrical power (W)
q''	Heat flux (W/m^2)
r	Radius (m)
Re	Reynolds Number
$S_{y,x}$	Standard error estimate
T	Temperature (°C)
V	Velocity (m/s)

Greek Letters and Symbols

Δ	Difference
$\dot{m}$	Mass flow rate (kg/s)
μ	Viscosity (kg/m-s)
ρ	Density (kg/m^3)
σ	Surface tension (N/m)
ψ	Change in set point temperatures (K)

Subscripts

Al	Aluminum
b	Bubble
e	Excess
exp	Experimental
f	Fluid
i	Inlet
j	Jet
l	Liquid
NB	Nucleate Boiling
sat	Saturation
SP	Single-phase
TP	Two-phase
v	Vapor
w	Wall

Chapter 1 – Introduction

1.1 Motivation

The dual motives of this study are to investigate potential solutions to the high heat output of electronics and to the desalination of saline water. Advancements in the electronics industry are resulting in electronic devices that require advanced cooling solutions to ensure safe operating temperatures. Development of high-efficiency small scale heat exchangers is necessary to dissipate heat generated by these electronic devices. To meet future demands, studies have focused on robust two-phase heat transfer devices.

The unavailability of safe drinking water is a problem faced by the inhabitants of impoverished countries. In particular, inhabitants of underdeveloped islands often have rainwater as their only source of potable water yet a limitless supply of salt water. A two-phase confined impinging jet is explored as a method of desalinating water.

1.2 Background

Continued investigation of innovative and efficient ways to dissipate heat from powered devices is needed to meet the cooling needs of the developing electronics industry. Small scale devices, such as microchannel heat sinks, have the potential for improved heat transfer performance. One of the drawbacks of small scale devices, however, is the increased pressure drop

required to move the fluid through the heat sink compared to conventional heat sinks.

For increased performance, heat may be dissipated by two-phase flow in order to take advantage of the energy required to change the phase of the working fluid. Two-phase flow in small scale devices, however, can create large pressure gradients and flow instabilities caused by the rapidly expanding vapor within the heat sink. In order to take advantage of two-phase flow while minimizing its disadvantages, the heat transfer performance of an axisymmetric impinging jet is investigated. Furthermore, confinement of the jet allows for an improvement of heat transfer due to recirculation within the confined gap region.

Chapter 2 – Literature Review

Small scale heat transfer devices present considerable advantages in performance compared to larger devices. Tuckerman and Pease showed that microchannel heat sinks are capable of dissipating 790 W/cm^2 [1]. The considerable pressure required to move the working fluid, however, discourages the use of microchannel heat sinks. To gain some of the benefits of small scale heat transfer devices while mitigating disadvantages, an impinging jet is considered.

2.1 Single-Phase Jets

The literature review of single-phase confined impinging jets is necessary to understand the influence that various parameters have upon the heat transfer. A review of single-phase impinging jets unrestricted by a confinement plate presented by Webb et al. [2] identifies the parameters that have the principal influence on heat transfer. These are the influence of gap height to nozzle diameter ratio, Reynolds number, and Prandtl number. The maximum heat transfer for unconfined impinging jets as a function of gap height to nozzle diameter ratio occurs when $H/d_j \approx 5$. This maximum is a result of turbulence generated by the jet increasing the effects of forced convection at the heating surface. The heat transfer is found to have a square root dependence on Reynolds number for unconfined jets. This effect is caused by the formation of a laminar boundary layer in the stagnation region [2].

For an area ratio of unity between the jet exit area and the gap inlet area the gap height to nozzle diameter ratio is equal to 0.25. Acceleration occurs between the outlet of the jet and the inlet of the channel when $H/d_j < 0.25$. For $H/d_j > 0.25$, deceleration occurs. At smaller H/d_j ratios, the effect of acceleration of the fluid has been shown by Chatterjee [3] to have an impact on heat transfer characteristics. Chatterjee [3] attributed this change to a distortion in the velocity distribution at the entrance plane of the gap and the subsequent development of enhanced vorticity generation when acceleration occurs. The strength of the primary vortex was shown to increase with decreasing H/d_j, thus increasing heat transfer. The secondary vortex was also shown to move closer to the stagnation point.

The introduction of a confinement surface to the study of single-phase jets adds complexity due to hydrodynamic interactions between the fluid and the confinement plate. The confinement surface creates recirculation which causes a decrease of the stagnation point heat transfer coefficient due to the breaking up of the jet [4]. However, recirculation vortices, also identified by He [5] and by Garimella and Rice [6], are believed to enhance the heat transfer coefficient downstream of the stagnation point.

Chang et al. [4] have proposed a single-phase heat transfer coefficient correlation for confinement geometries for $r_H/d_j > 1.25$ of the form

$$h_{SP} = \left(\frac{k_{Al}}{d_j}\right) 0.7017 Re_j^{0.574} Pr^{0.4} \left(\frac{H}{d_j}\right)^{-0.106} \left(\frac{r_H}{d_j}\right)^{-0.62} \tag{2.1}$$

This correlation considers the effects of parameters that were found to have significant influence on the single-phase heat transfer coefficient. Equation 2.1 was generated using R-113 as the working fluid over the range: 9500 ≤ $Re_j \leq 110{,}000$ and $1.5 \leq H/d_j \leq 4.0$.

Two additional correlations proposed for the single-phase heat transfer are presented. Li and Garimella [7] proposed that

$$h_{SP} = \left(\frac{k_{Al}}{d_j}\right) 0.690 Re_j^{0.555} Pr^{0.4} \left(\frac{L_j}{d_j}\right)^{-0.07} \left(\frac{2r_H}{d_j}\right)^{-0.348} \tag{2.2}$$

where L_j/d_j is the aspect ratio of the impinging nozzle. Their data was collected with water as the working fluid over the following range: $8500 \leq Re_j \leq 23{,}000$ and $1 \leq H/d_j \leq 5$. The Martin correlation [8] was developed from a review of single-phase impinging gas jets and is of the form

$$h_{SP} = G\left(A_r, \frac{H}{d_j}\right)\left(\frac{k_{Al}}{d_j}\right)\left[2Re_j^{1/2}(1 + 0.005Re^{0.55})^{1/2}\right] \tag{2.3}$$

where

$$G\left(A_r, \frac{H}{d_j}\right) = 2A_r^{1/2} \frac{1 - 2.2A_r^{1/2}}{1 + 0.2\left(H/d_j - 6\right)A_r^{1/2}} \tag{2.4}$$

where

$$A_r = \frac{d_j^2}{4r_H^2} \tag{2.5}$$

The correlation is applicable over the range: $2000 \leq Re_j \leq 400{,}000$ and $2 \leq H/d_j \leq 12$ and $0.004 \leq A_r \leq 0.04$. The three single-phase correlations

presented are considered in the development of a correlation describing the current experiment.

Thus far, the correlations presented have considered conditions where the fluid decelerates upon entering the gap as a result of the area change. A numerical analysis completed by Chattterjee [3] investigates the effects of the gap height to nozzle diameter ratio over the range $0.125 \leq H/d_j \leq 3$. Within this range, the gap height to nozzle diameter ratio was found to have drastic effects on the radial and axial velocities of the fluid entering the gap. In particular, for the case where flow accelerates between the jet outlet and gap inlet ($H/d_j = 0.125$), velocity trends were not similar to cases in which the acceleration did not occur. Though the analysis by Chatterjee [3] did not consider heat transfer, the gap height to nozzle diameter ratio was shown to have effect on vortex size and strength, which has been shown to effect the heat transfer performance of impinging jets [4, 5, 6].

2.2 Pool Boiling

Before two-phase impinging jet literature is presented, pool boiling is reviewed to introduce the effects of boiling on heat transfer. A review of saturated pool boiling will help to understand regimes of heat transfer as well as the underlying physical mechanisms of boiling. A review by Incropera et al. [9] identifies four basic boiling regimes: free convective boiling, nucleate boiling, transition boiling and film boiling. Free convective boiling occurs when the heating surface temperature is slightly above the saturation

temperature ($T_e \lesssim 5$ °C). In this regime, the creation of bubbles will occur; however, fluid motion is principally determined by the effects of free convection. The inception of bubbles becomes important in the nucleate boiling regime (5 °C $\lesssim T_e \lesssim$ 30 °C). In this regime, the heat transfer coefficient reaches a maximum value, which is a result of heat exchange to the liquid in motion at the surface. Transition and film boiling regimes occur at greater excess surface temperatures (30 °C$\lesssim T_e$), but are not reviewed in this study because test device limitations prohibit operation at these conditions.

As discussed by Incropera et al. [9], nucleate pool boiling can be considered a type of forced convection driven by bubble formation. As a result, the Nusselt number of the pool boiling correlation follows a common form for a forced convection correlation

$$\overline{Nu_d} = CRe_d^m Pr^n \tag{2.6}$$

where the constants C, m, and n are determined experimentally. Because the improved heat transfer coefficient is caused by rising bubbles, the appropriate characteristic length scale is the bubble diameter, D_b. The diameter of the bubble at departure can be thought of as a balance between surface tension and buoyant forces, and are often related by

$$D_b \propto \sqrt{\frac{\sigma}{g(\rho_l - \rho_v)}} \tag{2.7}$$

where σ is the surface tension, g is the gravitational constant, and ρ_l and ρ_v

are the saturated liquid and vapor densities, respectively. A characteristic velocity can be found by considering the distance the liquid must travel to replace the rising bubble and dividing by the time it takes for a new bubble to form, t_b. The time it takes for a bubble to form is equal to the energy it takes to form a bubble divided by the rate at which heat is added to the bubble [9]. The characteristic velocity can be represented by

$$V \propto \frac{D_b}{t_b} \propto \frac{D_b}{\left(\frac{\rho_l i_{fg} D_b^3}{q_s'' D_b^2}\right)} \propto \frac{q_s''}{\rho_l i_{lv}} \tag{2.8}$$

By substituting Equation 2.8 and Equation 2.7 into Equation 2.6, absorbing proportionalities into the constant C, and substituting Newton's law of cooling, the heat flux correlation for pool boiling, that was developed by Rohsenow [10], is

$$q_s'' = \mu_l i_{fg} \left[\frac{g(\rho_l - \rho_v)}{\sigma}\right]^{1/2} \left(\frac{c_{p,l}\Delta T_e}{C_{s,f} i_{fg} Pr_l^n}\right)^3 \tag{2.9}$$

The variables $C_{s,f}$ and n are experimentally determined and depend on the surface-fluid interface.

Pioro [11] experimentally evaluated $C_{s,f}$ and n for a variety of working fluids and heating surfaces and determined constants for a water and polished aluminum interface, $C_{s,f}$ = 0.011 and n = 1, and for a water and oxidized aluminum interface, $C_{s,f}$ = 0.011 and n = 1.26.

2.3 Two-Phase Jets

The heat transfer performance of two-phase impinging jets influenced by the effects of flow boiling. Literature identifies jet velocity, subcooling, gap height to nozzle diameter ratio, and heater diameter to jet diameter ratio as having significant impact on the heat transfer of two-phase confined impinging jets [12].

Wolf et al. [13] found the jet velocity to have greater effect on heat transfer of impinging jets at lower heat fluxes. This was also reported by Monde and Katto [14] who showed using a confined impinging jet of saturated water that the jet velocity had little influence in the nucleate boiling regime. Mudawar and Wadsworth [15] also performed confined impinging jet studies with FC-72 and found no change in the nucleate boiling region of the boiling curve based on changes in jet velocity.

The effect of subcooling upon boiling curves has been investigated. Mudawar and Wadsworth [15] found the nucleate boiling regime insensitive to changes in subcooling. Similar results were reported by Monde and Katto [14] who found that the effects of subcooling are only significant at lower heat fluxes. In the same study, Monde and Katto [14] also report the heat transfer to be independent of changes in the gap height to nozzle diameter ratio in the nucleate boiling regime.

The effect of the ratio of the heater width to slot width (w_H/w_N) was reported by Abishek et al [16]. The study numerically investigated the heat

transfer of a slot jet impinging on a surface using degassed water at 20 °C subcooling as w_H/w_N varied from 0.5 to 11. The effects of the heater width to slot width ratio were found to have significant impact upon the heat transfer of the confined slot jet. The heat transfer coefficient for small w_H/w_N is greater than for geometries with large w_H/w_N. This effect is considered in this study and is used to validate experimental results.

As presented in the impingement boiling review by Wolf et al. [12], the nucleate boiling regime of the boiling curve is similar to that of pool boiling. In the two-phase confined impinging jet correlation by Chang et al. [17], one parameter that is considered to shift the boiling curve is the Lockhart-Martinelli parameter at the inlet (χ), defined by Lockhart and Martinelli [18] as

$$\chi = \frac{\dot{m}_l}{\dot{m}_v}\sqrt{\frac{\rho_v}{\rho_l}} \tag{2.10}$$

which is used as a term to quantify two-phase interactions during flow boiling. Considering this influence, Chang et al. [17] have proposed that

$$h_{NB} = \left[\frac{\mu_f i_{fg}}{(\sigma/g\Delta\rho)^{1/2}}\right]\left(\frac{c_{p,l}}{C_{s,f} i_{fg} Pr_l^n}\right)^{3.5} T_e^{2.5} + h_{SP}[1.0 + 1.187\chi^{-0.438}] \tag{2.11}$$

and where

$$q'' = h_{TP} T_e \tag{2.12}$$

In the present study, because there is no vapor at the inlet, χ is infinite. This yields a single-phase heat transfer coefficient multiplier of one. Therefore, the correlation by Chang et al. [17] reduces to

$$h_{NB} = \left[\frac{\mu_f i_{fg}}{(\sigma/g\Delta\rho)^{1/2}}\right]\left(\frac{c_{p,l}}{C_{s,f} i_{fg} Pr_l^n}\right)^{3.5} T_e^{2.5} + h_{SP} \tag{2.13}$$

2.4 Surface Changes

During boiling, bubbles form where microscopic pockets of vapor are trapped in the roughness of the heating surface. These pockets, called nucleation sites, serve as inception locations for bubble formation. As a bubble expands, it will eventually depart from the surface and leave behind a small amount of vapor which will aid the formation of the next bubble. Yamagata et al. [19] showed that the heat transfer coefficient is augmented by the presence of many nucleation sites.

Under prolonged boiling, the number of nucleation sites caused by surface roughness greatly diminishes [9]. If there is a significant decrease in the number of nucleation sites, the heat transfer performance of a heating surface may decrease with prolonged boiling. This was seen by Ma and Bergles [20] who reported repeatability problems caused by surface changes over time. Their solution to prepare a repeatable surface was to heat-age the surface by boiling on it for 60 minutes; however, they found that this method did not produce the repeatability desired.

2.5 Desalination

A review of desalination by Shannon et al. [21] indicates that 1.2 billion people worldwide do not have access to safe drinking water. The problem of unavailability of safe drinking water is expected to become worse in the coming decades due to a global increase in potable water scarcity. A nutrition review by Sawka et al. [22] indicates that a daily water intake of 3.7 liters for adult men and 2.7 liters for adult women meets the needs of the majority of adults, although hot climates and strenuous physical activity can increase this need. Conventional methods of desalination exist and can reliably convert sea water or water from saline aquifers into potable water; however, these methods are often chemically and energetically intensive and require large systems [21]. The two most common methods of desalinating water are reverse osmosis and thermal distillation. Reverse osmosis involves the use of pumps to create a pressure differential to force liquid water through a semipermeable membrane [23]. Desalination by thermal distillation requires the heating of a saline solution in order to produce water vapor, which is then condensed to fresh water. Lattemann and Höpner [24] report that both of these desalination methods produce discharge water that contains chemical residues, which can kill marine life. Thermal distillation systems may also output biocides and antifoaming additives. As the demand for safe drinking water increases, more environmentally safe desalination methods will be required.

Membrane distillation is a relatively new method of desalination that has numerous advantages compared to current desalination technology. During the membrane desalination process, water is evaporated through a membrane and then condensed to fresh water. Lawson and Lloyd [25] report that key benefits of membrane distillation include lower operating pressures than pressure-driven membrane separation processes, reduced chemical treatment, and drastically reduced system size compared to thermal distillation processes. A well designed membrane desalination system is capable of water vapor fluxes of 75 kg/m^2-hr [25] which is comparable to water fluxes in reverse osmosis systems. Another report by Lawson and Lloyd [26] shows that the water vapor flux is proportional to the pressure change across the membrane. Water vapor flux is also seen to have a square root dependency on the temperature difference across the membrane.

Because boiling of the liquid is not required to desalinate the water, as is required for thermal distillation, the system can be operated at lower temperatures than the saturation temperature of the saline solution. Lawson and Lloyd [25] reported that typical operational temperatures for water in membrane distillation systems range from 60 °C to 90 °C and can be as low as 30 °C .This capability makes membrane desalination a method that can potentially incorporate a renewable energy source to power the system. Based upon the energy density required by membrane desalination systems, the most likely renewable energies to be paired with membrane desalination, as

published by Mathioulakis et al. [27] are geothermal and solar thermal. Solar thermal desalination systems have the capability of being operated anywhere there is sunlight and require less capital investment than establishing geothermal energy extraction.

Chapter 3 – Problem Statement

Review of current research of high efficiency compact heat sinks suggests that high heat transfer rates are attainable by microchannels and confined jet geometries. Two-phase flow is shown to have considerable heat transfer advantages compared to single phase flow in similar flow configurations. Research also suggests that heat flux, mass flux, and channel geometries can have a great effect on the operating temperature of the heat sink. Correlations have not yet been established for the performance of two-phase confined impinging jets with single phase inlet conditions for various parameters of heat flux, mass flux, and gap height to nozzle diameter ratio.

3.1 General Hypothesis

From previous research, heat flux has been shown to have a significant effect on the average surface temperature of two-phase confined impinging jets. A heat transfer correlation has been developed [17] for two-phase confined impinging jets with a two-phase inlet by characterizing the fluid inlet properties by the inlet quality. Based upon studies, which report surface temperature as a function of heat flux, gap height to nozzle diameter ratio, and mass flux, the effects of these parameters should be able to be quantified and correlated is a single equation.

3.2 Experimental Objectives

The heat transfer performance of the confined impinging jet will be evaluated by the excess temperature at the heating surface, T_e, and how it changes as a function of the three parameters of interest. These results will be compared to pool boiling correlations, single-phase confined jet correlations, and two-phase confined jet correlations in order to validate test results. Boiling curves comparing heat flux, q'', and excess temperature, T_e, will be used as a means of identifying the effects of varying the parameters of interest. As seen in previous investigations, the heat transfer coefficient of two-phase confined impinging jets can be approximated as the addition of a single-phase heat transfer component and a two-phase component. This will be the method employed in the development of a correlation as a function of the parameters of interest. Validation of data is accomplished by comparing data to other jet impingement studies with similar experimental conditions.

3.3 Tasks

The two main tasks for are the validation of experimental results and analysis of heat transfer performance. The validation of test data is critical to achieving the objectives of this study. The first step in the validation of the experimental results is to conduct a pool boiling experiment to compare the pool data to the Rohsenow [10] correlation. Using experimental data, variable constants of the correlation were evaluated in order to describe heat transfer characteristics of the surface-fluid interface. Finally, the pool data are

evaluated based on comparison to the Rohsenow [10] correlation and the variable constants were verified based on the results presented by Pioro [11]. The next step in validating experimental data was to ensure that the results collected correspond to a heating surface that does not change with time. Changes of the surface over time were assessed by taking the same set point thrice during a two hour experiment: once in the beginning, once after 50 minutes, and once again at the end of the experiment. Minimal changes of the excess temperature when all parameters are constant are evidence of a heating surface that is not changing with time.

Heat transfer performance of the jet is assessed by producing boiling curves for each of the experiments. By comparing test cases, the effects of the gap height to nozzle diameter ratio and the mass flux at the gap inlet on the excess temperature for a given heat flux can be determined. Using the two-phase correlations developed by Chang et al. [17] and Abishek et al. [16], performance trends for the experimental data can be evaluated. Deviations from these correlations are indicative of where parameters and conditions of the current study differ from those upon which the correlations are based.

Chapter 4 – Experimental Facility and Methods

The experimental facility used for testing allows for the variation of three parameters: applied heat flux, q''; mass flux at the gap inlet, G_i; and nozzle-to-surface spacing, H. Heat transfer performance is evaluated by computation of the surface temperature as a function of the parameters of interest. Discussion of the system is divided into three sections: test device, test facility, and data acquisition.

4.1 Test Device

The test device is designed to study confined impinging jets and allow for the variation of the three parameters of interest. It is required that the test device can be easily disassembled for cleaning and maintenance, can withstand high temperatures, and can seal completely in order that mass balances could be accurately evaluated. A two-piece housing, which holds all of the other components in place, was fabricated from Polyetheretherketone (PEEK). This material was selected for its high resistivity to thermal degradation. The two pieces fit together in a piston-cylinder arrangement that is sealed with an O-ring. During operation, the fluid flows through a jet in the middle of the upper housing, impinges on the heating surface, travels radially outwards into a vapor-liquid separation plenum, and exits the test device. Three borosilicate glass discs, sealed with an O-ring and spaced around the lower housing at equal intervals, are used to monitor the water level and hydrodynamic activity and to backlight the gap for high-speed

photography purposes. An extruded aluminum test stand secures the test device in place. A three-dimensional, exploded view of the test device is shown in Figure 4.1 to identify components and assembly.

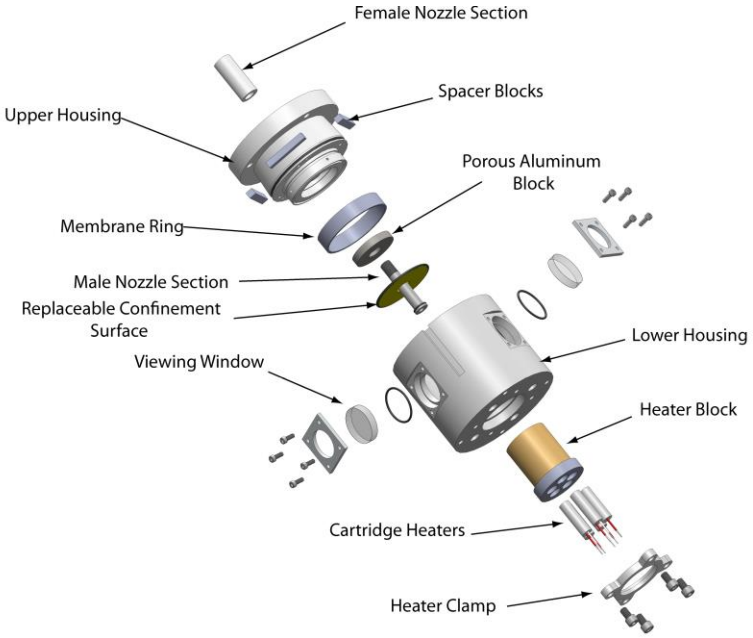

Figure 4.1: Exploded view of test device [28].

4.1.1 Heating Block

The heating block was fabricated from aluminum 6061 and contains cavities for the insertion of five 9.5 mm diameter, 300 W cartridge heaters and three shielded thermocouples. Figure 4.2 illustrates the depths and radial locations of the heater block cavities. The heating cartridges are secured in place with high-temperature RTV silicone to prevent movement during thermal cycling. The heating block is secured in place with a retaining clamp that bolts into the lower housing. When secured in place, the only portion of the heating block exposed to the fluid is the horizontal, circular

heating surface, which measures 38 mm in diameter. The method by which the heating surface is prepared is detailed later.

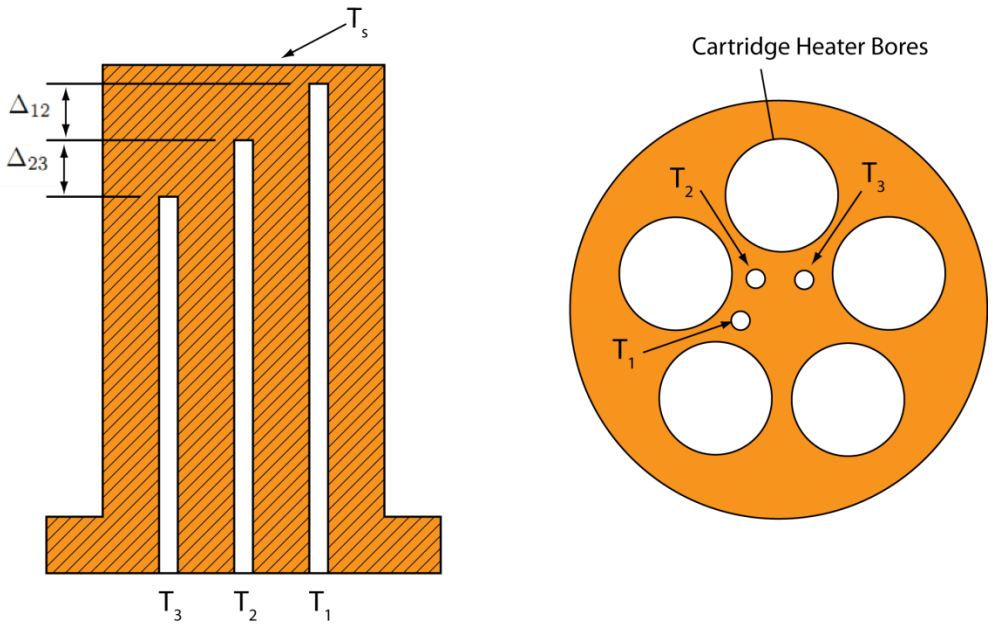

Figure 4.2: Illustration of thermocouple cavity depths in heater block (left) and radial positions of thermocouple and cartridge heater cavities (right) [28].

4.1.2 Confinement Surface

The test device is made to perform future tests where extraction can occur through a permeable Polytetrafluoroethylene (PTFE) membrane at the confinement surface. Because extraction was not considered in this study, the confinement surface is made impermeable with a swatch of non-porous PTFE. The non-porous membrane is supported with a polypropylene backing plate with square holes of 1 mm. An illustration showing a cross section of the confinement gap is presented in Figure 4.3. The PTFE membrane is attached to the upper housing by compressing it between a PEEK ring and the body of the upper housing. A seal is ensured by wrapping the upper

housing with PTFE thread seal tape prior to affixing the non-porous membrane and PEEK ring. To prevent the membrane from sagging onto the heating surface, a vacuum of 1-2 kPa gage is used to create a constant horizontal surface.

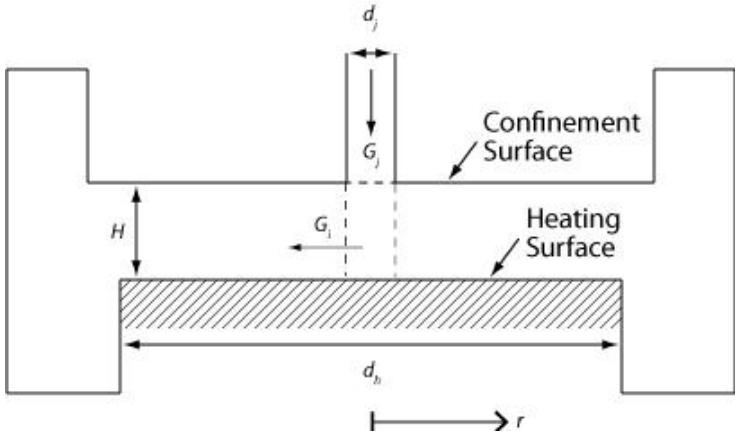

Figure 4.3: Cross-section of confinement gap.

4.1.3 Gap Height

The gap height in the device was maintained by the insertion of precision machined gage blocks between the lower and upper test device housings. The gage block heights for each required gap height were determined from precise measurements (±25 μm), taken at four points, of the depth of the heating surface below the lip of the lower housing.

4.2 Test Facility

In the following sections, the flow loop, instrumentation, and heater power supply used in this study are discussed.

4.2.1 Flow Loop

The flow loop is designed to transport distilled water to and from the test device. The flow loop is divided into two sections: one designed for the transport, filtering, and heating of liquid water and one designed for the transport, condensation, and collection of steam. During experimentation, the majority of the water in the system resides in the holding reservoir. The holding reservoir is a large metal container that can withstand the gas flame used for boiling the distilled water during the degassing process. While the experiment is being operated, the holding reservoir rests upon a Corning® Laboratory Stirrer/Hot Plate PC-220, which is set to the maximum heat setting.

The water is pumped from the holding reservoir to the test device with a Cole-Parmer® gear pump. Though the pump drive does have variable power controls, a needle valve is located downstream of the pump to more precisely control the mass flow rate. The distilled water is filtered through two 40 μm filters, installed in parallel, and one 1 μm filter. The water is heated by passing through a coiled tube inside a Neslab EX-7 hot oil bath. Further control of the subcooled temperature is achieved using rope heaters supplied with 3.9 watts. The subcooled inlet temperature is adjusted to the desired value by changing the hot oil bath temperature. The mass flow rate at the inlet is collected using a MicroMotion coriolis flow meter. The pressure and temperature of the inlet fluid are measured directly upstream of the inlet jet.

Liquid water leaves the test device through four outlet ports at the bottom of the lower housing. The liquid is pumped from the test device to the holding reservoir using a second Cole-Palmer pump and the outlet mass flow rate is recorded using a second MicroMotion coriolis flow meter.

The steam flow loop allows for the collection and reuse of vapor generated in the test device. During experimentation, vapor exits the test device through two outlet ports in the upper housing. Liquid water may also exit through these ports if the test device becomes completely flooded. Fluid that exits through these ports flows through a concentric tube heat exchanger and is collected in a beaker. The water in the collection beaker is periodically added to the reservoir.

4.2.2 Instrumentation

Temperature, pressure, and mass flow rate are recorded at several locations throughout the flow loop. Thermocouples used for temperature measurements were shielded T type. For fluid temperature measurements, one thermocouple was installed on the inlet T-fitting and one thermocouple was installed in the lower housing with the probe exposed to the outlet fluid pool. For heating block temperature measurements, three shielded, grounded, T type thermocouples are secured vertically in the heater block at the same radius and at various depths. The thermocouples range from 1.3 mm to 10.8 mm from the heating surface and are used to extrapolate the surface temperature. The thermal conductivity of aluminum 6061, k_{Al}, as

reported by the supplier, is 172 W/m-K. Using the thermocouple readings, thermal conductivity of the heating block, and distance from the heating surface, a one-dimensional application of Fourier's Law is used to determine the surface temperature at the radius at which the thermocouples are installed. A complete discussion of the determination of the surface temperature is presented in Chapter 5.

Pressure measurements are collected at three locations in the test device from three absolute pressure transducers with a range from 0 to 206 kPa. The pressure transducers were installed vertically with snubbers to prevent damage to the sensing elements. All three of the pressure transducers operate with an excitation voltage of 10 V, which is supplied with a Tektronix PG2125G programmable power supply. The fluid inlet pressure is recorded with a pressure transducer threaded into the inlet T fitting. The outlet pressure was measured from a port located on the upper housing immediately downstream on the confinement gap. The third pressure transducer records the absolute pressure supplied by the vacuum pump to adhere the PTFE membrane to the silicon support. Mass flow rate measurements are collected using two coriolis flow meters manufactured by MicroMotion and were installed in the liquid flow loop.

4.2.3 Heater Power Supply

Power is supplied to the five 300 W cartridge heaters by a custom power supply that was fabricated to safely control the power input. The power

supply requires a 240 volt, three-phase, 50 ampere electrical supply. A Watlow TemperatureLV controller operates a shutoff switch in the power supply that trips in the event of overheating of the heater block. The temperature threshold at which the power supply cuts power was set to 200 °C. The temperature probe used for this application is the middle heater block thermocouple. The voltage supplied to the cartridge heaters is controlled manually with a Powerstat variable autotransformer capable of delivering up to 1.5 kW. Fuses are installed between the power supply and cartridge heaters for an additional safety.

4.3 Data Acquisition

Two Dell workstations were used for data collection due to the number of signals collected and capability of the computers. The primary data acquisition computer collects temperature, pressure, and mass flow rate data using two National Instruments data acquisition cards. The data acquisition card used to collect mass flow rate and temperature measurements is an NI PCI-MIO-16E-4 with a 16 bit resolution and a 200 kilosamples per second maximum sampling rate. The data acquisition card used to collect pressure measurements is an NI PCI-6034E with a 12-bit resolution and a 250 kilosamples per second multichannel sampling rate. LabVIEW 2009 is used to collect measurements from both DAQ cards at a constant 3.5 Hz sampling rate throughout the entire experiment.

The secondary data acquisition computer collects the voltage and amperage delivered to the heating cartridges by the variable autotransformer. LabVIEW 2009 is used to communicate directly with a Tektronix THS720P Digital Real-Time Oscilloscope via an RS232 data cable. The oscilloscope displays amperage measurements using a Tektronix A261 current probe and voltage measurements using a Tektronix P5200 differential voltage probe. The differential voltage probe has two measurement ranges, 50x (0-150V) and 500x (150-1500V). The proper range is manually changed, as necessary, during experimentation. Sampling rate of the oscilloscope is approximately 0.87 Hz and is limited by the communication rate of the oscilloscope. The data at both workstations is recorded to the proprietary LabVIEW file format, technical data management solution (TDMS). The TDMS file format organizes data into a three-level hierarchy of objects in real-time.

The temperature values from the thermocouples are converted in LabVIEW by reference to a cold junction thermistor built into the DAQ board. The thermocouples secured in the heating block are grounded to improve signal to noise ratios. Pressure measurements are collected in terms of voltage values. Both temperature and pressure measurements are corrected from their raw form during processing using the calibration curves. Mass flow rates are collected from two coriolis meters in terms of frequencies. The frequencies are converted to mass flow rates using the scaling factor

$$F_{scale} = \frac{mass\ flow\ rate}{frequency}$$

where the mass flow rate corresponds to the flow rate scaling range, 800 g/min for this study, and the sampling frequency for the meters is 10 kHz.

Though data are collected throughout the entire operation of a test, steady-state data are identified manually. Steady-state data are data points that are marked during collection as points representative of the steady-state operating conditions of the experiment. This data collection is initiated when temperature measurements of the three thermocouples in the heater block do not change with time. Steady-state data is collected for approximately 1.5 minutes per test case at 3.5 Hz. Transient response times of the system vary based on test case conditions with an approximate range being less than 6.5 minutes for higher heat fluxes to greater than 10 minutes for lower heat fluxes.

Grounded and shielded connections are used for the pressure transducers. Removable connectors were installed on all pressure transducers and thermocouples to allow for easy disassembly of the test device. All connections were labeled to prevent confusion during reassembly.

4.4 Test Matrix

To assess the influence of heat flux, q'', mass flux at the gap inlet, G_i, and gap height to nozzle width ratio, H/d_j, on the performance of the confined impinging jet, a range of test conditions were developed from other confined

jet studies, initial testing, and facility limitations. Fixed testing conditions included a 4 mm diameter jet, 38 mm diameter aluminum heated impingement surface, and a working fluid of water with a subcooled inlet temperature of 10 °C. The test parameters are shown in Table 4.1. For each combination of G_i and H/d_j, a test was conducted where the surface temperature was collected at 10 different heat fluxes varying from 5 to 50 W/cm^2 in 5 W/cm^2 increments.

Table 4.1: Experimental testing parameters

Parameter	Values
H/d_j	0.125, 0.25, 0.5
G_i	200, 300, 400 kg/m^2-s
q''	5-50 W/cm^2

4.5 Test Procedure

The first step in the procedure consists of preparing the aluminum heating surface. The surface requires an enhanced preparation every three data sets. The enhanced preparation method consists of wet sanding the surface until it is visibly free of deposits. Next, the surface is cleaned with distilled water on a Kimtech® Kim-wipe. The surface is then wiped thoroughly: first with acetone, then isopropyl alcohol, and finally distilled water. Distilled water is degassed in the holding reservoir for approximately 30 minutes during the enhanced surface preparation process. Once degassed, the water is pumped through the flow loop and heated until it becomes a two-phase mixture. The fluid is then directed into the test device where

unconfined boiling occurs for 120 minutes at 25 W/cm^2. The prepared surface will maintain constant surface characteristics for three tests lasting 120 minutes apiece, at which point, the surface will need to undergo enhanced preparation again. Aside from enhanced surface preparation every three tests, the surface is prepared for each individual test by exposing it to air for at least 12 hours.

The distilled water is degassed by means of boiling for 30 minutes in the holding reservoir immediately before testing. To ensure steady mass flow rates, the flow loop filters are removed and back flushed to remove any deposits that may have collected during the previous test. During startup, the system mass flow rate is maintained as the oil bath and preheater settings are adjusted until the subcooled temperature is stabilizes at 10 °C. The cold water that flows through the concentric tube heat exchangers, serving to condense vapor, is turned on. An Air Cadet® vacuum/pressure pump is used to create a pressure differential across the non-porous PTFE membrane, causing it to press against the backing. Once the measured parameters in the flow loop have reached steady-state values, the data acquisition programs are initiated and testing begins.

During testing, the oil bath and needle valves are frequently adjusted to ensure that the subcooled temperature and mass flow rates, respectively, are maintained. For each power set point, the power supplied to the heating cartridges is adjusted with a variable autotransformer. Once the heating

surface temperature has stabilized, steady-state data is collected. The first data case for each experiment is conducted at 20 W/cm^2. This set point is also repeated again during the incremental power increase from 5 to 50 W/cm^2.

The final data case is also collected at 20 W/cm^2. This set point is collected thrice in order to observe how the heat transfer performance changes across the time scale of the experiment. Once the final data case is collected, all heat input devices are turned off and the system is allowed to cool until all system temperatures drop below 90 °C. At this point, the pumps and all instruments are turned off and the test device is immediately disassembled.

Chapter 5 – Data Reduction and Analysis

The process by which data is collected, processed, and used in order to determine heat transfer performance is detailed in this chapter.

5.1 Data Reduction

During data collection, two dedicated data acquisition (DAQ) computers simultaneously collect relevant measurements using LabVIEW measurement software by National Instruments. The primary computer collects temperature, pressure, and mass flow rate measurements and the secondary computer collects measurements of the power supplied to the heating cartridges. The data from the primary computer is stored in LabVIEW's TDMS file format and is converted to a Matlab file using code supplied by National Instruments. Next, calibration curves are applied to the raw data. During processing, checks are made to ensure that there are no spurious data and that the test cases collected from the two computers corresponded with each other. Finally, the Matlab file containing the temperature, pressure, and mass flow rate data is combined with the processed voltage and amperage data collected as a text file from the secondary DAQ computer.

5.2 Performance Analysis

The raw power delivered to the heater block is calculated from the voltage and amperage recorded by the oscilloscope, by the relation

$$q_P = VI \tag{5.1}$$

The uncorrected heat flux is then found from

$$q_P'' = \frac{q_P}{A_H} \tag{5.2}$$

Because some of the raw power leaves the heater block through surfaces other than the heating surface, the raw power and heat flux must be corrected.

To determine the losses that occur during operation, a 2.5 cm thick piece of PTFE was machined to fit snuggly onto the heating surface and act as an insulator. Subcooled water of 10 °C was circulated through the outlet plenum to simulate experimental conditions. Power was supplied to the heater block in increments of 5 W and the heater block temperatures were recorded. Data was recorded until the surface temperature reached the maximum temperature reached in experiments. By assuming that no heat traveled through the PTFE block, an equation could was developed relating power losses to heater block temperature. A linear fit was applied to the data and the following power loss equation

$$q_{loss} = 0.4135 \times T_{HB_2} - 35.3 \tag{5.3}$$

was developed to evaluate losses during experimentation. The variable T_{HB_2} is the thermocouple reading as recorded by the middle thermocouple.

Once q_{loss} was quantified, the corrected heat flux could be found from

$$q_{PC}'' = \frac{VI - q_{loss}}{A_s} \tag{5.4}$$

where q_{PC}'' is the heat flux applied at the surface corrected for losses.

The heating surface temperature is extrapolated using a 1-D application of Fourier's Law evaluated for each thermocouple. An example of this calculation using the thermocouple farthest from the surface is

$$T_w = T_3 - \frac{q''_{PC}}{k_{Al}\Delta_{3s}} \tag{5.5}$$

where Δ_{3s} is the distance between the thermocouple location and the surface. Initially, this analysis was performed for each thermocouple. The wall temperature as determined by the middle thermocouple was found to be consistently different than the temperatures extrapolated by the thermocouples closest to and farthest from the heating surface. As a result, the wall temperature, T_w, used in this experiment is an average of the extrapolated values using the first and third thermocouples in the heater block. The excess surface temperature

$$T_e = T_w - T_{sat} \tag{5.6}$$

is evaluated using the extrapolated wall temperature and the saturation temperature. The saturation temperature, along with all other saturated fluid properties, is calculated using the XSteam Matlab program and evaluated based on the average pressure between the inlet and exit of the gap.

5.3 Uncertainty

The uncertainty analysis follows the methodology outlined by Figliola and Beasley [29]. The uncertainty of measured values was evaluated for each

instrument. Thermocouples and pressure transducers were calibrated with a linear fit. The standard error estimate for a linear fit is defined as

$$S_{x,y} = \sqrt{\frac{\sum y_1^2 - b\sum y_1 a\sum x_1 y_1}{n-2}} \tag{5.7}$$

where a and b are the coefficients of the least-squares line fit to the calibration data and n is the number of points in each calibration curve. The bias error of a measurement is then evaluated as

$$\Theta_{bias} = \sqrt{S_{x,y}^2 + U_{stnd}^2} \tag{5.8}$$

where U_{stnd} is the published uncertainty of the measuring instrument. The precision error associated with repeated measurement was evaluated as

$$\Theta = \sqrt{\Theta_{bias}^2 + (t_{95} \times \sigma)^2} \tag{5.9}$$

where σ is the standard deviation of the repeated measurements, not to be interpreted as the surface tension previously defined, and t is the student T-statistic for a 95% confidence interval [29]. The calculated uncertainty is calculated from propagating the measurement uncertainty using the Kline and McClintok method, which is defined as

$$U_R = \sqrt{\sum_{i=1}^{n} \left(\frac{\partial R}{\partial x_i}\Theta_i\right)^2} \tag{5.10}$$

where R is a functional relation dependent upon the variables x_1,x_2,…x_n. A sample calculation is presented in Appendix A and representative values are also shown as error bars on boiling curve plots.

Chapter 6 – Results and Discussion

In order to be confident about the data obtained from experimentation, data were validated by several methods. This chapter is divided into three sections: validation of experimental data, results of the data analysis, and application of this technology to the desalination process.

6.1 Validation

The collected data was validated three different ways. The first validation, without which no other validations could be made, was to ensure that the heating surface maintained surface characteristics throughout an experiment. It is also required that the surface characteristics are repeatable from test to test. The second validation was to determine the constants characterizing the surface and compare those to published data. Finally, initial results were validated by comparison to research by Abishek et al. [16].

6.1.1 Surface Repeatability

Prolonged saturated pool boiling of water on the polished aluminum surface has been shown to change the surface characteristics over time [20]. At a heat flux of 25 W/cm^2, the average surface temperature was recorded to change as much 3.5 °C over 190 minutes at an approximately constant rate. The heating surface temperature of a sanded and cleaned aluminum surface decreases rapidly for the first 40 to 60 minutes and then steadily increases for the remainder of the prolonged boil, as is seen in Figure 6.1. Pictures of

the surface before and after prolonged boiling are shown in Figure 6.2. The black surface resulting from prolonged boiling is caused by both oxidation and mineral deposits. Wet sanding the surface completely removes deposits.

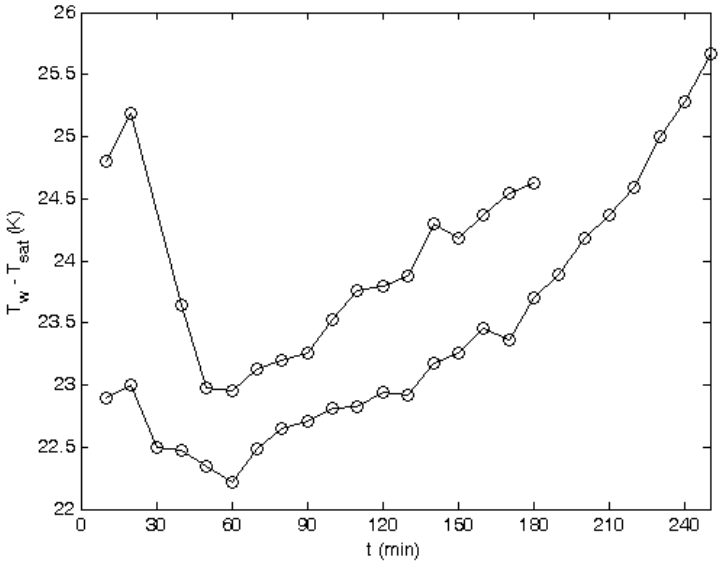

Figure 6.1: The excess temperature of the heating surface during two constant 25 W/cm^2 heat flux pool boiling tests as a function of time.

Figure 6.2: Photographs of the heating surface taken before (left) and after (right) 240 minutes of boiling at 25 W/cm^2.

Through trial and error, it was discovered that neither sanding nor cleaning the heating surface after boiling, coupled with exposing the surface to air for at least 12 hours, produced a surface that had more constant characteristics over time than a freshly sanded and cleaned surface. Through iteration, a method was developed that produced a surface with repeatable surface characteristics over the duration of an experiment, approximately 120 minutes. The results of this method were initially assessed by boiling degassed, distilled water with the heating surface at 25 W/cm^2 for approximately 120 minutes. Figure 6.3 shows the changes in the excess surface temperature of the heating surface during the preparation boil and two boiling cases following the preparation. All cases were conducted at a surface heat flux of 25 W/cm^2. Between cases, the surface was exposed to air for at least 12 hours. As can be inferred from the figure, the preparation method prepares a surface that can undergo boiling for an extended period of time with minimal and anticipated changes of the surface temperature. Figure 6.4 shows a photograph of the surface after a 120-minute test using the described surface preparation method.

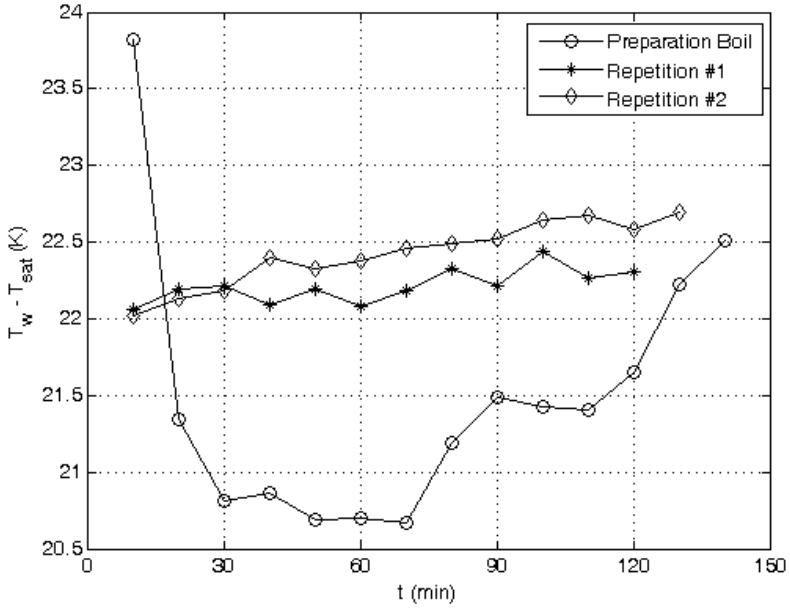

Figure 6.3. Changes in the excess surface temperature over time for the preparation boiling case and two repeated boiling cases at 25 W/cm^2.

Figure 6.4: Heating surface prepared with the described surface preparation method after a 120-minute test.

The change in surface characteristics during an experiment is quantified by comparing the computed surface temperature at a given heat flux, gap height to nozzle diameter ratio, and mass flux between two set points before

and after an experiment. With the developed method, the surface temperature changed by an average of 0.7 °C during experimentation, with a maximum of 1.4 °C, which occurred for one test. Figure 6.5 shows difference in temperature between the two 20 W/cm^2 set points before and after every test as a function of how many times the same surface had been used. It is observed that variation of the surface temperature during an experiment generally increases with the number of times a surface is used. Therefore, it was determined that a prepared surface should only be used for three, 120-minute experiments, at which time it should be sanded and cleaned again.

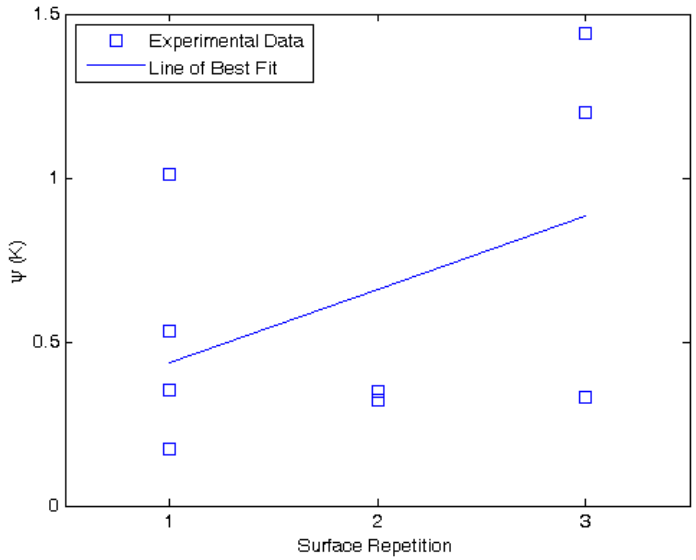

Figure 6.5: Change in excess temperature between two 20 W/cm^2 test cases collected before and after testing. $\psi = T_{e,final} - T_{e,initial}$

6.1.2 Determination of Surface Characteristics

Once the constancy of the heating surface could be verified, saturated pool boiling was simulated and surface characteristics for the prepared

aluminum surface were determined. The method of least squares was used to determine the two surface-fluid interface constants used in the Rohsenow [10] correlation to be $C_{s,f}$ = 0.017 and n = 1.22. The determined value of the constant $C_{s,f}$ is similar to that found by Sabo [28], who used the same experimental facility and working fluid and a similar heating surface. For a water/aluminum interface Pioro [11] determined $C_{s,f}$ to be 0.011. Differences in these values may be the result of the way in which pool boiling was simulated in this study. The n value determined is in the range of the two n values found for the two water/aluminum interface experiments published by Pioro [11]: 1.20 and 1.26. The experimental data overlaid with the Rohsenow [10] correlation using the two determined constants is presented in Figure 6.6.

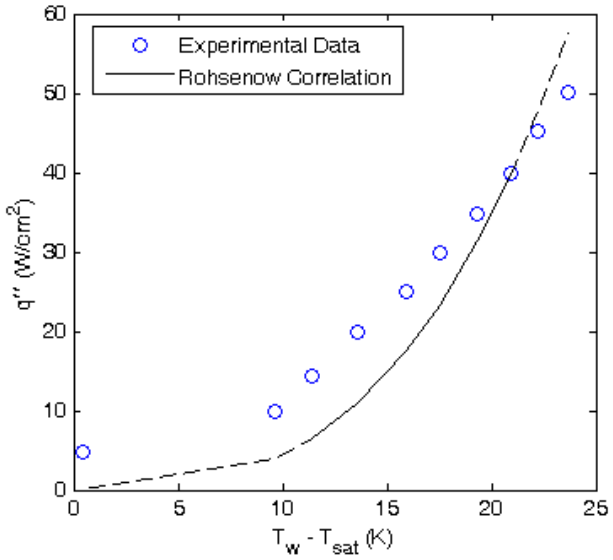

Figure 6.6: Experimentally acquired pool boiling data and the Rohsenow [10] correlation. Dashed lines indicate an extrapolation of correlation.

The greatest discrepancy between the Rohsenow [10] correlation with empirical surface constants and the experimental data is at lower heat fluxes, which under predicts the heat flux for a given surface temperature. This difference could be the result of a pool that was not completely saturated. Though a two-phase inlet was used to replenish the pool with saturated water, the small reservoir may have been subcooled due to heat loss to the environment. A subcooled pool could explain deviations from the correlation at lower surface excess temperatures. This would also explain why the correlation is more accurate at higher heat fluxes; the effects of a subcooled working fluid are only significant at low heat fluxes [12]. A second explanation for why the experimental data matches the correlation poorly at lower heat fluxes is because, as discussed in Chapter 2, the Rohsenow [10] correlation was developed as a model of forced convection caused by nucleate boiling. As a result, the correlation is not applicable to the free convection boiling regime.

6.1.3 Comparison to Correlations

The final step of validation was to compare initial test results to other two-phase confined impinging jet data. As shown computationally by Abishek et al. [16], the heater width to nozzle width ratio, w_H/w_j, can have significant impact on the heat transfer coefficient. Their boiling curve results were used to validate the initial results of the current study because the heater width to nozzle width ratio of the current study falls within the range of d_H/d_j values

investigated by Abishek et al. [16]. Furthermore, both studies were conducted with subcooled, two-phase water as the working fluid. Figure 6.7 shows the comparison between the boiling curves collected by Abishek et al. [16] and the boiling curve of this study with a jet Reynolds number most similar to their study.

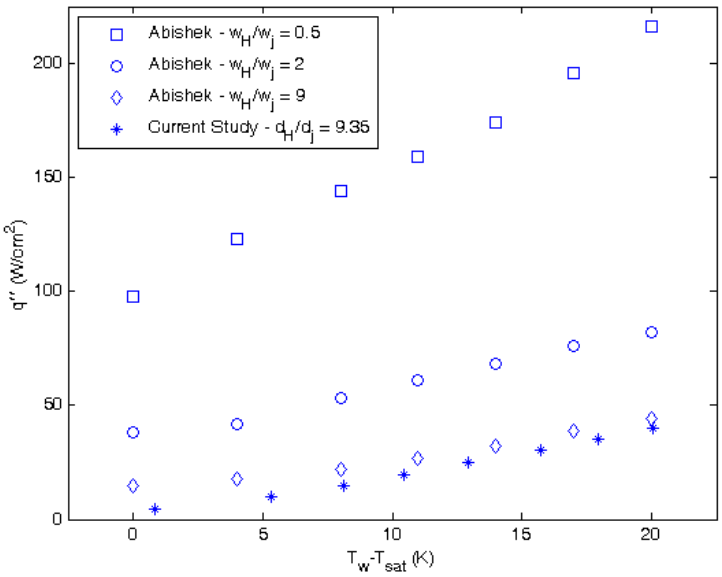

Figure 6.7: Comparison of boiling curves by Abishek et al [16] to boiling curve of current study. (Re_{w_j} = 2500 [16] vs. Re_{d_j} = 2800)

The boiling curve collected in this study is similar to that recorded by Abishek et al. [16] for a similar heater width to nozzle width ratio. The boiling curve for the current study departs from the boiling curves by Abishek et al. [16] near lower heat fluxes. This indicates that the influence of the subcooled working fluid is lower in the current study, which is to be expected because a subcooled inlet temperature of 10 °C was used while Abishek et al. [16] used a subcooled inlet temperature of 20 °C. In general, the current

boiling curve is similar to that of the two-phase confined impinging jet with subcooled water at the inlet data presented by Abishek et al [16].

6.2 Experimental Results

Trends in the heat transfer performance are presented through the use of boiling curves which are used to develop a correlation relating heat flux to parameters of interest.

6.2.1 Boiling Curves

Boiling curves were generated for each test case to assess the effects of the parameters of interest. The influence of the mass flux at the gap inlet is illustrated in Figure 6.8 and Figure 6.9 for H/d_j of 0.5 and 0.25, respectively. As is evident from the boiling curves, the effect of mass flux causes small shifts of the boiling curve, but trends remain similar. The same independency is not seen for $H/d_j = 0.125$ where mass flux does appear to have a significant effect at higher heat fluxes, as presented in Figure 6.10.

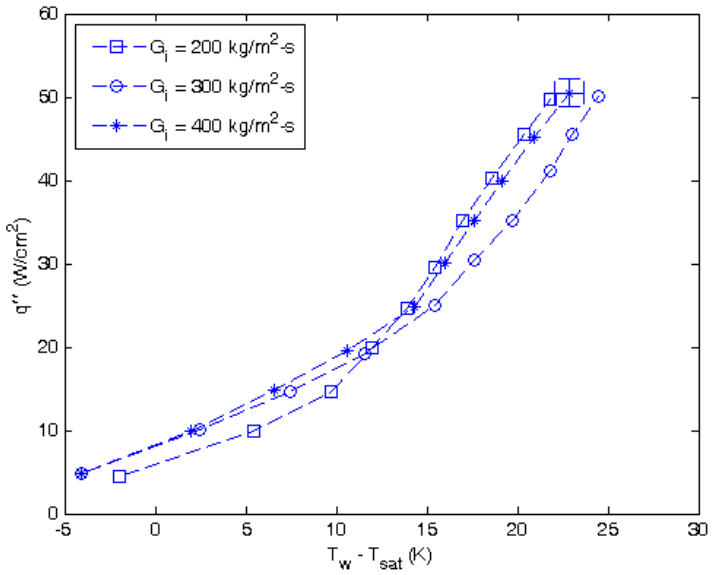

Figure 6.8: Effects of mass flux at the gap inlet for a fixed gap height to jet diameter ratio of 0.5. A representative error bar is shown for measurements of excess temperature and heat flux.

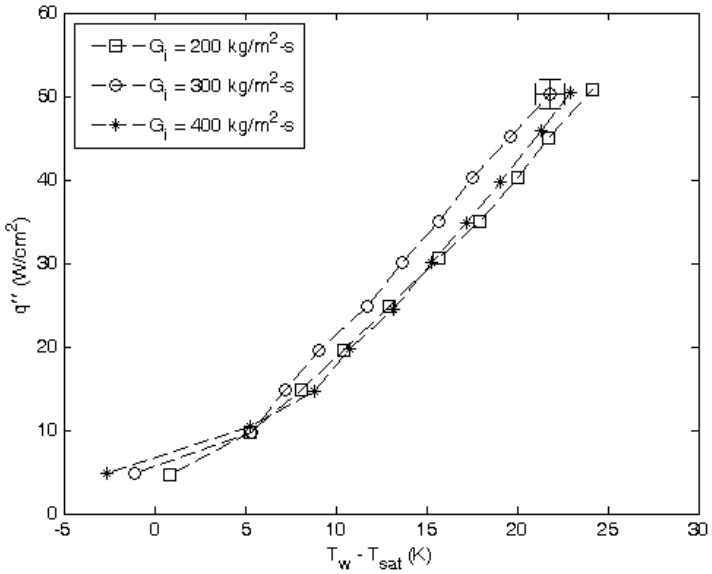

Figure 6.9: Effects of mass flux at the gap inlet for a fixed gap height to nozzle diameter ratio of 0.25.

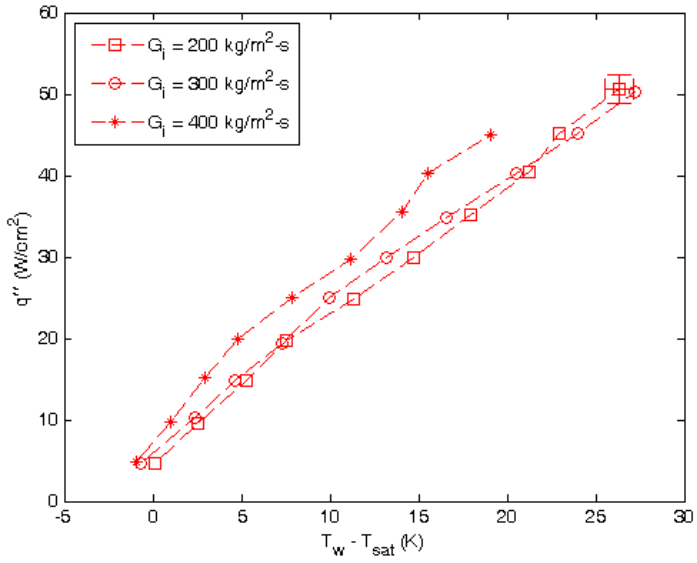

Figure 6.10: Effects of mass flux at the gap inlet for a fixed gap height to nozzle diameter ratio of 0.125.

The influence of the gap height to nozzle diameter ratio on the heat transfer performance is presented in Figure 6.11 to Figure 6.13 for mass fluxes at the gap inlet of 400, 300, and 200 kg/m^2-s, respectively. Judging from the boiling curves, it is apparent that trends for H/d_j = 0.125 do not match trends for other gap height to nozzle diameter ratios. While typical boiling curves are concave up for the free convection and isolated bubble nucleate boiling regimes, trends for H/d_j = 0.125 show a convex boiling curve suggesting significant improvements in the heat transfer coefficient for small excess wall temperatures. Also noticed is that the H/d_j = 0.125 boiling curves have lower operating wall temperatures for a given heat flux compared to the other boiling curves, especially in the free convection and isolated bubble nucleate boiling regimes.

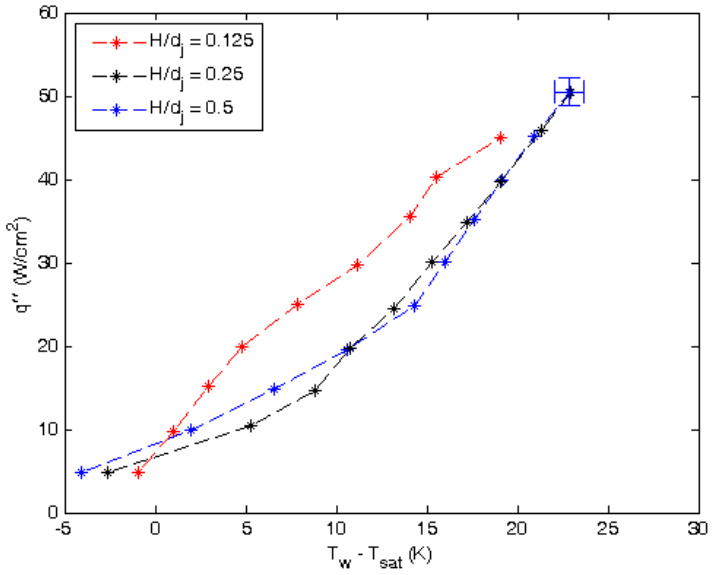

Figure 6.11: Effects of gap height to nozzle diameter ratio for a fixed mass flux of 400 kg/m^2-s at the gap inlet.

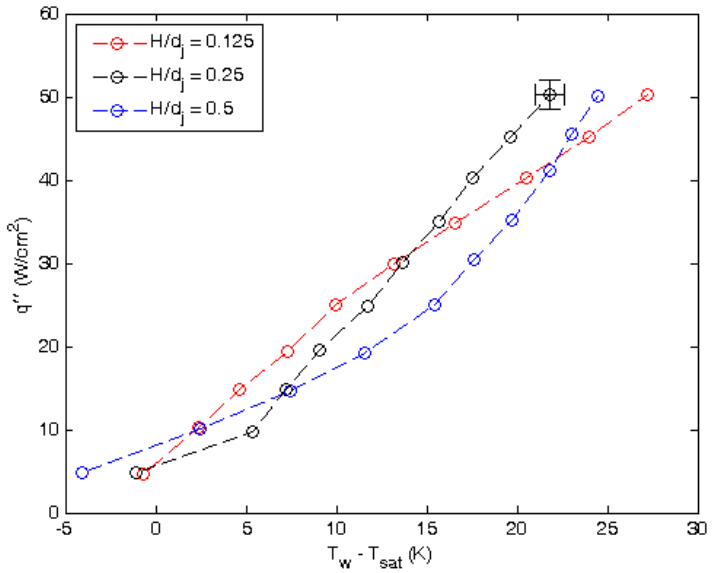

Figure 6.12: Effects of gap height to nozzle diameter ratio for a fixed mass flux of 300 kg/m^2-s at the gap inlet.

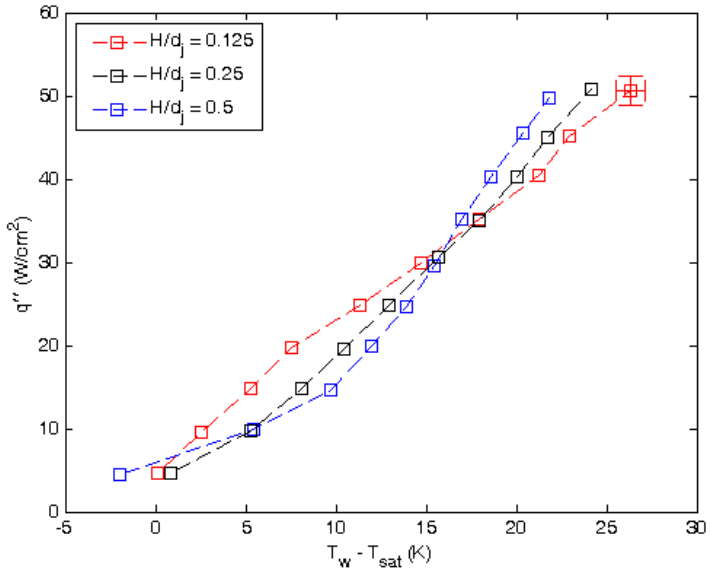

Figure 6.13: Effects of gap height to nozzle diameter ratio for a fixed mass flux of 200 kg/m^2-s at the gap inlet.

Based on the literature review, there are two possible explanations for the occurrence of atypical boiling curves when the gap height to nozzle diameter ratio is 0.125. The first is due to fluid acceleration between the outlet of the nozzle and inlet of the gap. For gap height to nozzle diameter ratios of 0.25 and 0.5, the area of the gap inlet is equal to and twice that of the area of the jet outlet, respectively. As shown by Chatterjee [3], acceleration of the fluid in this region can have significant effects on the velocity profile of the fluid that are not present otherwise. This would explain why changes in the gap height to nozzle diameter ratio are especially significant at a value of 0.125. This is the only gap height to nozzle diameter ratio for this present study where a positive acceleration of the fluid velocity occurs upon entering the gap.

A second explanation for why the boiling curves for a gap height to nozzle diameter ratio of 0.125 are different than the typical boiling curve is because different heat transfer phenomena may be occurring. As was presented by Incropera et al. [9], boiling can be thought of as a type of forced convection initiated by liquid replacing the void left behind by the bubble leaving the surface. As mentioned in Chapter 2, this theory was the basis of the derivation of the Rohsenow [10] correlation, which has been shown to describe the two-phase effects of confined impinging jets for the nucleate boiling regime [28]. At the smallest gap height to nozzle diameter ratio, when H = 0.5 mm, the gap height is expected to be on the same scale as the bubble diameter; D_b = 0.5 mm [5]. While boiling still is occurring, the mechanisms of bubble departure and quenching may be drastically different. If the mechanisms of boiling are being changed by the similar scale of the gap height and bubble diameter, the heat transfer performance may well depart from the predicted boiling curve based on bubbles leaving the heating surface as a result of buoyancy forces.

6.2.2 Correlation Development

The correlation provided by Chang et al. [17] served as the model by which a correlation was developed that considered the parameters of interest of this study. The first step was to determine the exponent of the excess temperature term, T_e. While Yamagata et al. [19] showed that, for nucleate

boiling, heat flux, q'', is proportional to surface excess temperature to the third power, T_e^3, the exponent may change once flow boiling is introduced.

Chang et al. [17] report that the nucleate boiling contribution can be represented as

$$q''_{NB} = \left[\frac{\mu_f i_{fg}}{(\sigma/g\Delta\rho)^{1/2}}\right]\left(\frac{c_{p,l}T_e}{C_{s,f} i_{fg} Pr_l^n}\right)^m \tag{6.1}$$

where m is computed from experimental data. Recalling that the correlation by Chang et al. [17], is of the form

$$q''_{TP} = q''_{SP} + q''_{NB} \tag{6.2}$$

Equation 6.1 and Equation 6.2 can be substituted and rearranged to be of the form

$$\frac{q''_{TP} - q''_{SP}}{\left[\frac{\mu_f i_{fg}}{(\sigma/g\Delta\rho)^{1/2}}\right]} = \left(\frac{c_{p,l}T_e}{C_{s,f} i_{fg} Pr_l^n}\right)^m \tag{6.3}$$

By taking the natural logarithm of each side and moving the exponent, m, to be a constant, a linear relationship of the form

$$\ln\left(\frac{q''_{TP} - q''_{SP}}{\left[\frac{\mu_f i_{fg}}{(\sigma/g\Delta\rho)^{1/2}}\right]}\right) = m \times ln\left(\frac{c_{p,l}T_e}{C_{s,f} i_{fg} Pr_l^n}\right) \tag{6.4}$$

develops between the two logarithmic terms. Using experimental data, the two terms are plotted in Figure 6.14. A linear regression that is forced through the origin is displayed on the plot. This is done because the form of the linear relationship derived in Equation 6.4 passes through the origin.

The linear fit, forced through the origin, has a slope of 4.0, which indicates that heat flux has a fourth power dependence on excess surface temperature. This also indicates that the nucleate boiling heat transfer coefficient has a third power dependence on excess surface temperature.

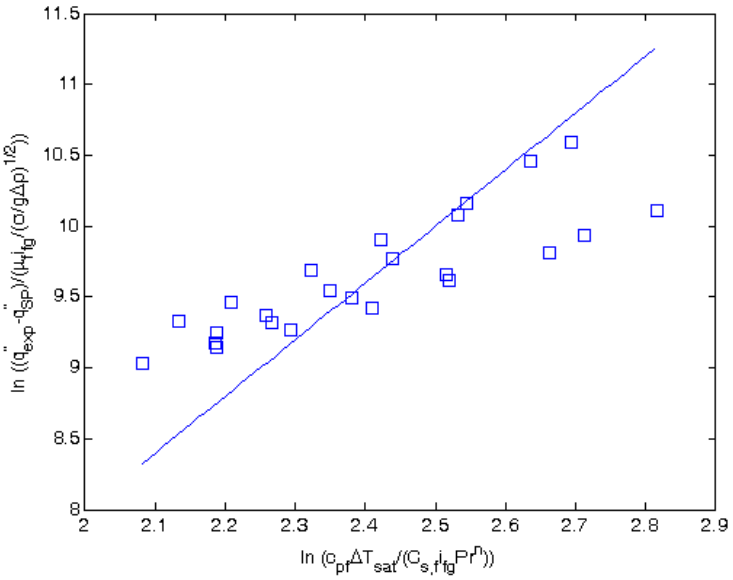

Figure 6.14: Linear fit of nucleate boiling data used to determine exponent of excess temperature term in correlation.

Considering the evaluated exponent of the excess temperature term, the modified form of the two-phase heat transfer becomes

$$h_{NB} = \left[\frac{\mu_f i_{fg}}{(\sigma/g\Delta\rho)^{1/2}}\right]\left(\frac{c_{pf}}{C_{s,f} i_{fg} Pr^n}\right)^4 (T_e)^3 \qquad (6.5)$$

The parameters of gap height to nozzle diameter ratio and mass flux at the inlet were considered by including two more terms with the two-phase heat transfer correlation, one for each parameter. The multiplier term for the gap height to nozzle diameter ratio is $\left(H/D_j\right)^a$ and the multiplier term for the

mass flux is $\left(G_i/G_{i,max}\right)^b$. For dimensional consistency, the mass flux is scaled by the maximum mass flux of this experiment, $G_{i,max}$ = 400 kg/m^2-s. The variables a and b were evaluated using the least squares method with two degrees of freedom. The values compared in the least squares analysis were the measured heat flux and calculated heat flux using the proposed correlation. Including these terms, the proposed two-phase heat transfer coefficient is

$$h_{NB} = \left[\frac{\mu_f i_{fg}}{(\sigma/g\Delta\rho)^{1/2}}\right]\left(\frac{c_{pf}}{C_{s,f} i_{fg} Pr^n}\right)^4 (T_e)^3 \left(\frac{H}{D_j}\right)^{-0.51} \left(\frac{G_i}{G_{i,max}}\right)^{-0.58} \quad (6.6)$$

The accuracy of the proposed correlation can be visually assessed in Figure 6.15. With only three exceptions, test cases with a gap height to nozzle diameter ratio of 0.25 and 0.5 are correctly predicted with an accuracy of ±25%. Gap height to nozzle diameter ratios of 0.125 are not well predicted with this correlation as can be seen in Figure 6.16. This was anticipated from the atypical boiling curves produced by tests at this gap height to nozzle diameter ratio. A more traditional scaling parameter of the Reynolds number at the gap inlet was considered instead of G_i/G_{max}, however, this method did not collapse the data as well. The results of a correlation using the Reynolds number are presented in Figure 6.17.

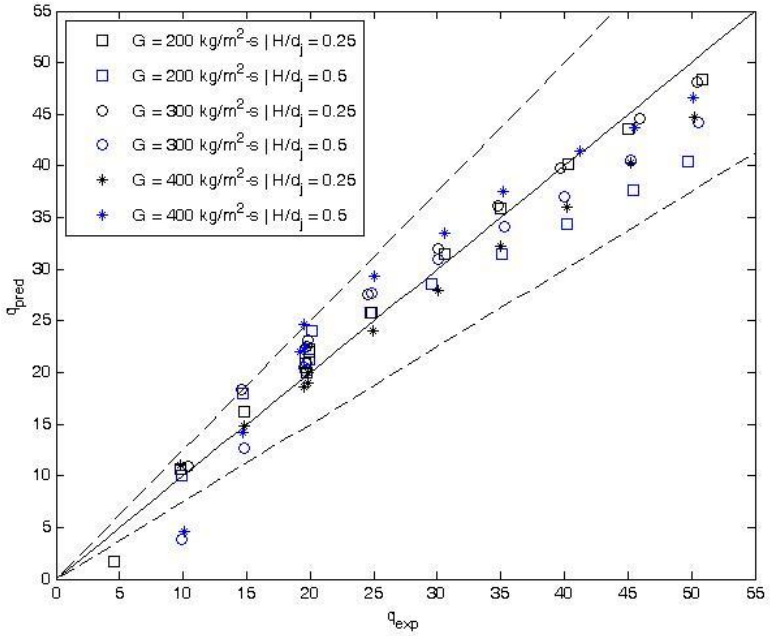

Figure 6.15: Comparison of experimentally determined heat flux to predicted heat flux using proposed correlation. Dashed lines are ±25% uncertainty.

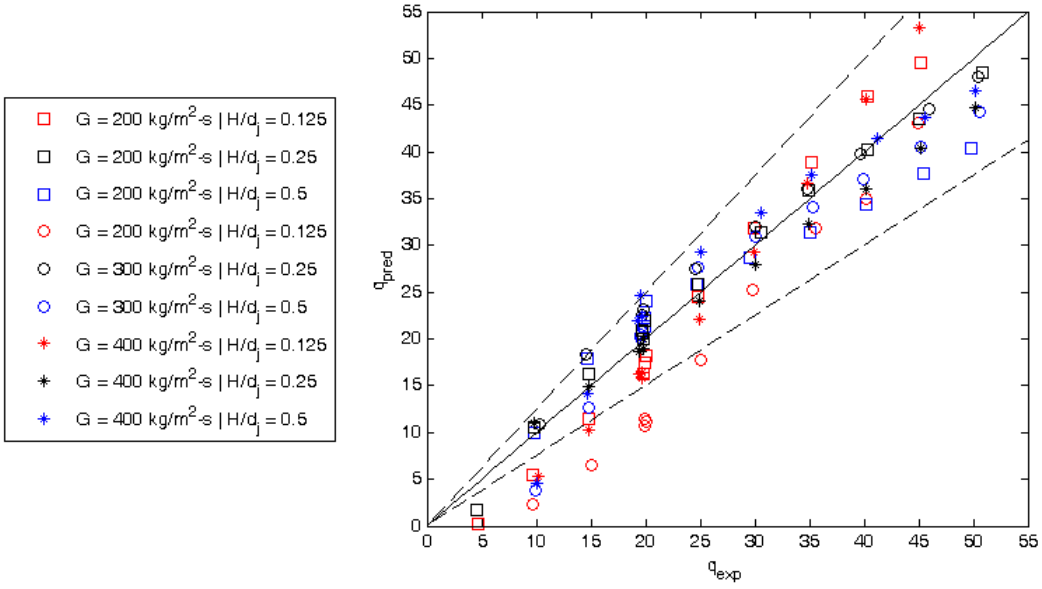

Figure 6.16: Comparison of experimentally determined heat flux to predicted heat flux using proposed correlation including points where $H/d_j = 0.125$.

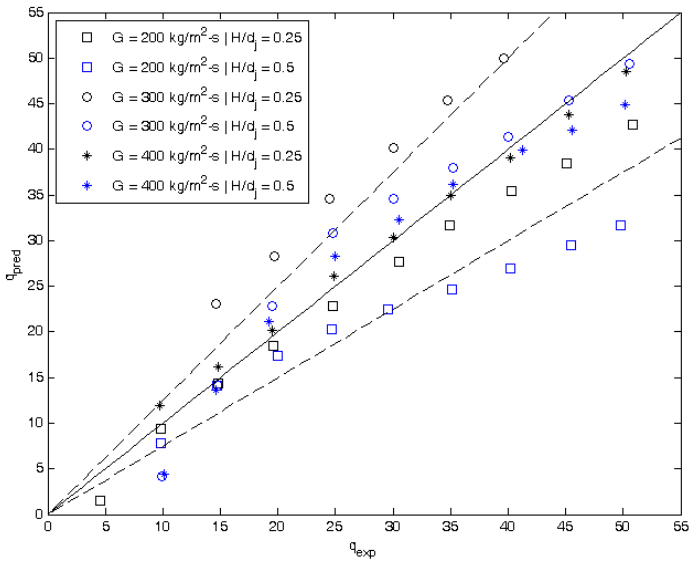

Figure 6.17. Comparison of experimentally determined heat flux to predicted heat flux using a correlation including the Reynolds number at the gap inlet.

6.3 Desalination Application

The jet configuration for two-phase heat transfer application, retrofitted with a hydrophobic porous membrane at the confinement surface, allows for the combination of membrane desalination and thermal distillation system. One advantage of using the current jet configuration for membrane desalination is that the small gap heights would be particularly useful for this process due to the large membrane surface area exposure per unit volume of saline water. The small gap height is also beneficial to desalination because it would reduce the thermal gradient between the heating surface and the confinement surface. The disadvantage of membrane desalination, however, is the limits in water vapor flux through the membrane.

The advantage of thermal distillation is that it overcomes the water vapor flux limit of membrane desalination because water vapor flux through the surface is caused by both evaporation and extraction of vapor produced in the gap. This would allow for increased production of fresh water when needed. Though the current experimental setup used distilled, filtered water, deposits were still left behind on the surface after prolonged boiling. Despite the deposition of mineral deposits on the heating surface, it was noted that there were no deposits on the non-porous PTFE membrane. This is an early indication that operation of a membrane desalination system as a thermal distillation system would not introduce deposits within the pores of the membrane that would decrease the permeability of the membrane.

A final advantage of desalination by means of vapor extraction is the enhanced rate of water vapor flux across the membrane. The existing facility has demonstrated water vapor fluxes of 20 grams of water vapor per minute through 580 mm^2 of porous PTFE. This rate of extraction was the maximum observed when a pressure drop of 30 kPa was applied across a membrane with pore sizes of 0.45 μm and with a confinement plate to heating surface spacing of 2 mm. This is equal to a water flux of 2,080 kg/m^2-hr, a twenty-seven fold increase from the typical water flux for a well-designed conventional membrane desalination system. With the current facility operating at the extraction test conditions, the daily water needs of a family of four could be produced in 3.2 hours. This production rate, however,

requires that 950 watts be supplied to the heating surface. Though this energy demand is large, it would be attainable by concentrating solar radiation with a parabolic disc reflecting the light onto the backside of the heating surface. For example, using a parabolic reflector with a reflectivity of 90% and a heating surface with an absorptivity of 90% on its backside, the area of the parabolic disc required would be 0.84 m^2. For this experiment, electric vacuum pumps were used to extract vapor from the confinement region; however, a 30 kPa pressure drop across the membrane could be easily achieved with the use of a hand or foot pump. Finally, this analysis considers a replication of conditions for the one extraction test. Fortunately, the rate of extraction would likely increase with a smaller confinement plate to heating surface spacing and a membrane with larger pore sizes.

The primary drawback of operating the device as a thermal distillation system is a decrease in heat transfer performance that would be experienced while boiling due to mineral deposits on the heated surface. The results of the present study, however, provide limitations for how long and under what conditions boiling can be performed to prevent degradation of the heat transfer capabilities of the surface. If a combination membrane desalination and thermal distillation system is to be researched, the results of this study suggest an upper limit of duration for which the facility could be operated at maximum fresh water production rate. However, as discussed previously, the

impinging jet offers the ability for the device to be used as an efficient membrane desalination system as well.

Chapter 7 – Conclusion and Recommendations

A conclusion of the findings is presented and recommendations for future investigations inspired by this study are provided.

7.1 Conclusion

The current study was motivated by the demand for high heat transfer cooling solutions and the need for efficient desalination. The heat transfer performance of two-phase confined impinging jets was examined using experimentally obtained results. In this study, the average operating temperature of the heat sink as a function of heat flux, inlet mass flux, and gap height to nozzle diameter ratio were investigated. Heat transfer performance is presented using boiling curves and is compared to existing correlations.

The test configuration consists of a 4 mm diameter jet of water, entering the jet inlet at a subcooled temperature of 10 °C. The jet impinges on a 38 mm diameter heated aluminum surface then flows radially outward within a confined gap. Experimental parameters include inlet mass fluxes ranging from 200 to 400 kg/m^2-s, confinement gap height to nozzle diameter ratios from 0.125 to 0.5, and input heat fluxes from 5 to 50 W/cm^2. Conditions of the heater surface were found to strongly influence heat transfer performance.

A method was developed that allows for the preparation of an aluminum surface with repeatable and stable surface characteristics. The method involves wet sanding the heating surface; cleaning the surface with distilled water,

acetone, isopropyl alcohol, and then distilled water again; boiling distilled, degassed water on the surface for 120 minutes at 25 W/cm^2; and then exposing the surface to air for at least 12 hours in order to dry. The prepared surface can be used for three, 120-minute tests between which the surface is exposed to air for at least 12 hours. After three, 120-minute tests, the surface preparation method must be repeated.

Boiling curves indicate that the effects of the mass flux on the heat transfer performance were significant at low input heat fluxes and were minimal at high heat fluxes where the heat transfer coefficient is dominated by two-phase phenomena. The gap height to nozzle diameter ratio is seen to have little effect on the heat transfer performance for values of 0.25 and 0.5. When the ratio is 0.125, however, the heat transfer performance varies significantly from compared to other test cases. This difference is attributed to phenomena caused by either flow acceleration between the jet outlet and gap inlet and/or the similarity in scale between the gap height and bubble diameter. Using experimentally determined surface-fluid interface characteristics, a correlation was developed relating the heat flux to the parameters of interest. The developed correlation predicts the measured heat flux within ±25%.

7.2 Recommendations

The surface characteristics of an aluminum surface undergoing prolonged water boiling were shown to change over time. While a method was developed

to prepare a repeatable surface, the method limits experiment duration to 120 minutes and requires sanding the surface, which changes the physical dimensions of the heater block and may influence experimental results. A different heating surface material that could undergo prolonged boiling without inducing changes of the surface characteristics would allow for longer and more complex tests to be conducted with greater reliability.

The locations of the thermocouples in the heater block limits the accuracy with which the average surface temperature can be known. By varying the radii at which the thermocouple probes are situated would allow for an identification of radial changes in the surface temperature and a better prediction of the average surface temperature.

The current study suggests that either the gap height to nozzle diameter ratio or the gap height or both parameters can induce significant changes to the boiling curves when small. A study that explores the individual variation of these parameters would elucidate causes of shifts in the boiling curves.

The boiling curves for the impingement jet show a diminished performance than anticipated by other studies. This is attributed to a large heater diameter to nozzle diameter ratio. Ideally, future studies would allow for the variation of this parameter.

Another parameter of interest that could be introduced to an expanded study of two-phase confined impinging jets is the effect of extracting vapor through the confinement plate. Extraction would potentially allow for

decreased pressure drop and a delay of the critical heat flux. Extraction would also allow for the test device to operate as a desalination system to investigate the performance of a combination membrane desalination and thermal distillation system.

Bibliography

[1] D. B. Tuckerman and R. Pease, "High-performance heat sinking".

[2] B. Webb and C. Ma, "Single-phase liquid jet impingement heat transfer," *Advances in Heat Transfer,* vol. 26, pp. 105-217, 1995.

[3] A. Chatterjee, "Newtonian Radial Entrance Flow," *American Institute of Chemical Engineerins Journal,* vol. 46, no. 3, pp. 462-475, 2000.

[4] C. Chang, G. Kojasoy, F. Landis and S. and Downing, "Confined single- and multiple-jet impingement heat transfer--I. Turbulent submerged liquid jets," *International Journal of Heat and Mass Transfer,* vol. 38, no. 5, pp. 833-842, 1995.

[5] X. He, "CFD Simulation of Single-Phase and Flow Boiling in Confined Jet Impingement with in-Situ Vapor Extraction Using Two Kinds of Multiphase Models," Oregon State University, Corvallis, 2013.

[6] S. Garimella and R. Rice, "Confined and submerged liquid jet impingement heat transfer," *Journal of Heat Transfer,* vol. 117, no. 4, pp. 871-877, 1995.

[7] C. Li and S. Garimella, "Prandtl-number effects and generalized correlations for confined and submerged jet impingement," *International Journal of Heat and Mass Transfer,* vol. 44, no. 18, pp. 3471-3480, 2001.

[8] H. Martin, "Heat and mass transfer between impinging gas jets and solid surfaces," *Advances in Heat Tranfer,* vol. 13, 1977.

[9] F. Incropera, D. DeWitt, T. Bergman and A. Lavine, "Pool Boiling," in *Fundamentals of Heat and Mass Transfer*, John Wiley & Sons, Inc., 2007, pp. 624-642.

[10] W. Rohsenow, "A method of correlationg heat transfer data for surface boiling of liquids," *Transactions of American Society of Mechanical Engineers,* 1952.

[11] I. Pioro, "Experimental evaluation of constants for the Rohsenow pool boiling corelation," *International Journal of Heat and Mass Transfer,* vol. 42, no. 11, pp. 2003-2013, 1999.

[12] D. I. F. a. V. R. Wolf, "Jet Impingement Boiling," *Advances in Heat Transfer,* vol. 23, pp. 1-132, 1993.

[13] D. Wolf, F. Incropera and R. Viskanta, "Local jet impingement boiling heat transfer," *International Journal of Heat and Mass Transfer,* vol. 39, no. 7, pp. 1395-1406, 1996.

[14] M. Monde and Y. Katto, "Study of burn-out in a high heat boiling system with an impinging jet (part 1, behavior of the vapor-liquid flow)," *Trans. JSME,* vol. 43, pp. 3399-3407, 1977.

[15] I. Mudawar and D. Wadsworth, "Critical heat flux from a simulated dhip to a confined rectangular impinging jet of dielectric liquid," *International Journal of Heat and Mass Transfer,* vol. 34, no. 6, pp. 1465-1479, 1991.

[16] S. Abishek and R. N. V. Narayanaswamy, "Effect of heater size on confined subcooled jet impingement boiling," in *Proceedings of the ASME 2012 Summer Heat Transfer Conference*, 2012.

[17] C. Chang, G. Kojasoy, F. Landis and S. and Downing, "Confined single- and multiple-jet impingement heat transfer - II. Turbulent two-phase," *International Journal of Heat and Mass Transfer,* vol. 38, no. 5, pp. 843-851, 1995.

[18] R. Lockhart and R. and Martinelli, "Proposed correlation of data for isothermal two-phase, two-component flow in pipes," *Chemical Engineering Progress,* vol. 45, no. 1, pp. 39-48, 1949.

[19] K. Yamagata, F. Kirano, K. Nishiwaka and H. Matsuoka, "Nucleate boiling of water on the horizontal heating surface," *Mem. Fac. Engng.,* 1955.

[20] C. Ma and A. Bergles, "Jet impingement nucleate boiling," *International,* vol. 29, no. 8, pp. 1095-1101, 1986.

[21] M. Shannon, P. Bohn, M. Elimelech, J. Georgiadis, B. Mariñas and A. Mayes, "Science and technology for water purification in the coming decades," *Nature,* vol. 452, pp. 301-310, 2008.

[22] M. Sawka, S. Cheuvront and R. Carter, "Human water needs," *Nutrition Reviews,* vol. 6, no. 2, pp. 30-39, 2005.

[23] M. Elimelech and W. Phillip, "The Future of Seawater Desalination: Energy, Technology, and the Environment," *Science,* vol. 333, no. 712, pp.

712-717, 2011.

[24] S. Lattemann and T. Höpner, "Environmental impact and impact assessment of seawater desalination," *Desalination,* vol. 220, pp. 1-15, 2007.

[25] K. Lawson and D. Lloyd, "Membrene Distillation," *Journal of Membrane Science,* vol. 124, pp. 1-25, 1997.

[26] K. Lawson and D. Lloyd, "Membrane distillation. II Direct contact MD," *Journal of Membrane Science,* vol. 120, pp. 123-133, 1996.

[27] E. Mathioulakis, V. Belessiotis and E. Delyannis, "Desalination by using alternative energy: Review and state-of-the-art," *Desalination,* vol. 203, pp. 346-365, 2007.

[28] M. Sabo, "Performance and Flow Stability Characteristics in Two-Phase Confined Impinging Jets," Oregon State University, Corvallis, 2012.

[29] R. Figliola and D. Beasley, Theory and Design for Mechanical Measurements, Hoboken: John Wiley & Sons, Inc., 2011.

Appendices

Appendix A – Uncertainty Calculations

Sample calculations of the uncertainty of the experimental results are provided to demonstrate how the heat flux and surface temperature uncertainties are evaluated. Values used for the following sample calculations were selected from a representative data set and are included. The uncertainty for each measurement is found from a combination of the bias and precision errors using Equation 5.9.

The corrected heat flux is evaluated as

$$q''_{PC} = \frac{IV - Q_{loss}}{A_s} \tag{A.1}$$

where Q_{loss} is determined from Equation 5.3. An application of the Kline and McClintok method shows that the total uncertainty is

$$U_{q''_{PC}} = \sqrt{\left(\frac{\partial q''_{PC}}{\partial I} U_I\right)^2 + \left(\frac{\partial q''_{PC}}{\partial V} U_V\right)^2 + \left(\frac{\partial q''_{PC}}{\partial A_s} U_{A_s}\right)^2 + \left(\frac{\partial q''_{PC}}{\partial Q_{loss}} U_{Q_{loss}}\right)^2} \tag{A.2}$$

where

$$U_{A_s} = \frac{\partial A_s}{\partial d} U_d \tag{A.3}$$

and

$t_{95} = 1.960$

$d = 3.8$ cm

$I = 3.962$ Amps

$V = 139.4$ Volts

$Q = 592.9$ Watts

$Q_{loss} = 21.07$ Watts

$U_d = \sqrt{(0.00254)^2 + t_{95} \times (0.00254)^2}$

$U_d = 0.0044$ cm

$U_{A_s} = \frac{d}{2\pi} U_d$

$U_{A_s} = 0.0027$ cm^2

$U_I = \sqrt{(0.01)^2 + t_{95} \times (0.0080)^2}$

$U_I = 0.0150$ Amps

$U_V = \sqrt{(0.5)^2 + t_{95} \times (0.2526)^2}$

$U_V = 0.6124$ Volts

$U_{Q_{loss}} = 2.14$ Watts

$$U_{q''_{PC}} = \sqrt{\left(\frac{V}{A_s} U_I\right)^2 + \left(\frac{I}{A_s} U_V\right)^2 + \left(\frac{VI - Q_{loss}}{A_s^2} U_{A_s}\right)^2 + \left(\frac{1}{A_s} U_{Q_{loss}}\right)^2}$$

$U_{q''_{PC}} = 3.397$ W/cm^2

The uncertainty in the surface temperature was calculated assuming a 3% uncertainty in material properties.

$$T_{wall} = T_{HB2} - q''_{PC} \frac{k}{L_{2w}}$$

$$U_{T_{wall}} = \sqrt{\left(\frac{\partial T_{wall}}{\partial q''_{PC}} U_{q''_{PC}}\right)^2 + \left(\frac{\partial T_{wall}}{\partial k} U_k\right)^2 + \left(\frac{\partial T_{wall}}{\partial L_{2w}} U_{L_{2w}}\right)^2 + \left(\frac{\partial T_{wall}}{\partial T_{HB2}} U_{T_{HB2}}\right)^2}$$

$T_{2W} = 123.2$ °C

$q''_{PC} = 50.42$ W/cm^2

$L_{2W} = 0.576$ cm

$k_{Al} = 172$ W/m-k

$U_{L_{2W}} = \sqrt{(0.00254)^2 + t_{95} \times (0.004)^2}$

$U_{L_{2W}} = 0.00606$ cm

$U_{T_{HB2}} = \sqrt{(0.9)^2 + t_{95} \times (0.524)^2}$

$U_{T_{HB2}} = 1.161$ °C

$$U_{T_{wall}} = \sqrt{\left(\frac{k}{L_{2W}} U_{q''_{PC}}\right)^2 + \left(\frac{q''_{PC}}{L_{2W}} U_k\right)^2 + \left(\frac{q''_{PC}}{L_{2W}^2} U_{L_{2w}}\right)^2 + \left(U_{T_{HB2}}\right)^2}$$

$U_{T_{wall}} = 1.6$ °C